CrossMark

ORIGINAL PAPER

Influence of shear rheometer measurement systems on the rheological properties of microfibrillated cellulose (MFC) suspensions

Michel Schenker (iD) · **Joachim Schoelkopf** · **Patrick Gane** · **Patrice Mangin**

Abstract Flow curve and viscoelastic measurements were performed on microfibrillated cellulose (MFC) suspensions of different solids content using both cylinder and cup (smooth and rough) as well as vane in cup geometries. To compare the data quantitatively from amplitude sweep measurements and dynamic flow curves several descriptors were newly introduced to parameterize the observed two-zone behaviour separated by a transition region. It was observed that the cylinder cup geometries are prone to erroneous effects like slip, wall depletion and/or shear banding. However, those effects were not observed when the MFC suspension was not stressed beyond the dynamic critical stress (yield) point, i.e. when still in the linear viscoelastic regime. The vane in cup system on the other hand, seems to be less affected by flow inhomogeneities. By following the rheological properties as a function of the MFC suspension solids content, it could be shown that the global property trends remained alike for all investigated measurement systems, despite the presence of erroneous effects in some geometries. The observed effects were linked to recent model hypotheses in respect to the morphology of MFC suspensions under changing shear situations.

Keywords Microfibrillated cellulose (MFC) · Rheology · Vane · Depletion layer · Flow curve · Viscoelasticity

M. Schenker · P. Mangin
University of Quebec in Three Rivers (UQTR), 3350
Boulevard des Forges, Trois-Rivières, QC G9H 5H7,
Canada
e-mail: patrice.mangin@uqtr.ca

M. Schenker (✉)
FiberLean Technologies Ltd., Par Moor Centre, Par Moor
Road, Par, Cornwall PL24 2SQ, England, UK
e-mail: michel.schenker@fiberlean.com

M. Schenker · J. Schoelkopf · P. Gane
Omya International AG, Baslerstrasse 42, 4665 Oftringen,
Switzerland
e-mail: joachim.schoelkopf@omya.com

P. Gane
e-mail: patrick.gane@omya.com

P. Gane
Department of Bioproducts and Biosystems, School of
Chemical Engineering, Aalto University,
00076 Aalto, Helsinki, Finland

Introduction

Since 1983, when microfibrillated cellulose (MFC) was introduced by Turbak et al. (1983), extensive work has been carried out on the manufacturing, modification, application and metrology of this versatile material (Desmaisons et al. 2017; Kangas et al. 2014; Nechyporchuk et al. 2016a). The versatility originates from two main factors; on the one hand, various types of source materials can be used, including virtually all types of plants and even animals (tunicates), whilst on the other hand, there are several manufacturing processes, including diverse pre- and post-treatments that also lead to very different morphologies of the final product. Despite several attempts, there is still no unified nomenclature for all the different cellulose types, yet commonly used differentiations are fibrillated versus crystalline (Nechyporchuk et al. 2016a) and nano- versus micro-sized width (Moon et al. 2011). The differentiation between nanofibrillated- and microfibrillated cellulose (NFC and MFC, respectively) is not made very consistently in the literature, where the classical meaning of micro is re-emerging to cover the nano region. In this context, Kangas et al. (2014) should be referenced as it provides a straightforward definition, stating that only materials containing solely nano-sized fibrils (related to fibril widths) should be called NFC. MFC materials may also contain nano-sized fibrils, yet they also contain larger fibrils or even fibres, so they have a broad particle width-distribution ranging up to the micrometre-scale. The material investigated in this work is therefore classified as MFC.

With the increasing level of commercialization of MFC materials, the need increases also for meaningful methods of characterization. On the one hand, they are needed for quality control, and, on the other hand, a good differentiation of various grades is needed to be able to select an optimal product for a specific application. Several attempts at classifying properties have been made lately (Desmaisons et al. 2017; Kangas et al. 2014), concluding that a combination of several different methods is needed. A rather direct characterization is particle size analysis. However, due to the naturally high aspect ratio of cellulose fibrils, the broad distribution of length and widths and their tendency to coil, such analyses become rather challenging. The only direct method providing actual fibril dimensions, like width and length, is image analysis. The need for extensive sample preparation, long measurement times and the requirement for many counts to achieve statistical relevance, render such characterizations impractical. So, an easier characterization method, that would still provide some information on the fibril morphology would be very interesting.

The rheology of suspensions is known to depend inter alia on the size features of the suspended phase, so it might be a good candidate. Also, it is comparatively fast and generally does not need large sample volumes for a measurement. Not surprisingly, quite some work on the rheological characterization of various nano- and micro-cellulose suspensions has already been carried out. Very commonly, flow curves (viscosity as a function of shear rate) and viscoelastic properties are determined. Typically, rheology is often used as an additional characterization, but without a specific property target discussion (Dimic-Misic et al. 2016; Naderi et al. 2016; Padberg et al. 2016; Pahimanolis et al. 2013). Yet still, and especially lately, more and more work can be found, that specifically investigates the rheology of nano- and micro-cellulose suspensions (Dimic-Misic et al. 2015, 2017; Iotti et al. 2011; Martoïa et al. 2016; Nazari et al. 2016; Nechyporchuk et al. 2016b). A major topic in this field is the presence of rheometric-induced artefacts (side-effects) like wall depletion (migration of the fibrils away from the measurement cell walls), shear banding and wall slip (Haavisto et al. 2011; Kumar et al. 2016; Naderi and Lindström 2016; Nechyporchuk et al. 2014, 2016b; Saarinen et al. 2014). These effects can contribute significantly to the measurement data and, therefore, lead to misinterpretations. So, it is very important to minimize such effects as much as possible, or at least be aware and consider them in model developments. It was found that the type of rheometer and the type of measurement system can influence these perturbing effects, and, therefore, the resulting measured properties (Nechyporchuk et al. 2014; Saarinen et al. 2009). Nechyporchuk et al. (2014) have shown, that the side-effects also depend on the type of cellulose, i.e. that MFC types (named as "enzymatic-NFC" by the authors) are even more prone to side-effects. Several researchers concluded that parallel-plate and cone-plate setups of shear rheometers may lead to even more secondary effects (Naderi and Lindström 2015; Nazari et al. 2016; Saarinen et al. 2009), and so the use

of wide gap concentric cylinder (CC) set-ups is recommended. Other counter measures include rough and serrated surfaces or vane in cup geometry. However, what is still missing even now is a direct comparison of the commonly mentioned counter-measures against these side-effects with view to the more susceptible MFC suspensions. The present work aims to fill this gap and to provide some insights on the efficiency of those counter measures, as well as relate the specific system characteristics to prevailing hypothesized structural models of MFC suspensions (Karppinen et al. 2012; Saarikoski et al. 2012).

Several researchers also use pipe and/or slit rheometer setups to investigate the flow dynamics of MFC suspensions, often coupled with additional techniques that allow a tracking and/or visualization of the fibril structures (Haavisto et al. 2011, 2015; Kataja et al. 2017; Kumar et al. 2016; Lauri et al. 2017). An ad hoc comparability of data obtained by shear and pipe/slit-rheometers is not to be expected as the deformation is initiated by mechanical shearing via two surfaces on the one hand, whereas on the other hand it is pressure driven. Yet, several authors were able to show that comparability of the different resulting datasets is given under some conditions (Haavisto et al. 2015), or through respective data handling/treatment (Haavisto et al. 2017). Using pipe/slit rheometers can have several advantages, for example the reduced likelihood of restricting floccu-lation, or the ability to add several different measure-ment techniques in parallel (Haavisto et al. 2015; Kataja et al. 2017). However, a rather large amount of sample material is necessary for such volumetric flow setups (typically $> 1 \, dm^3$), and potentially changing suspension morphologies along the measurement tube due to extended residence time as a function of tube length (Haavisto et al. 2015).

Four different rheometer measurement systems are compared in this study, including two smooth CC set-ups with different measurement gaps, one rough surface CC setup and a vane in cup setup. A further aim of this work is to propose some new descriptors to classify the properties that can be gathered from flow curve and amplitude sweep data that allow a more quantitative analysis of the observations, in particular, the typically reported three-region shape of the flow curve (Iotti et al. 2011; Jia et al. 2014; Karppinen et al. 2012; Saarikoski et al. 2012; Shafiei-Sabet et al. 2012)

is parameterized as two zones separated by a transition region.

Methods

Materials

MFC was manufactured by a purely mechanical process, described in detail elsewhere (Schenker et al. 2016). In short, bleached eucalyptus pulp was mechanically disintegrated as a 3 wt% aqueous suspension (tap water) using a Supermasscolloider MKCA 6-2 (Masuko Sangyo Co., Japan) in various single passes at different rotational speeds. The specific grinding energy, defined as the total electrical energy consumption normalized by the amount of dry cellulose matter, was 7.2 kWh kg^{-1}. This mechanical fibrillation process typically leads to a broad size distribution (Lauri et al. 2017), i.e. coarse fibres as well as individual fibrils are present in such a suspension (Fig. 1). It is, therefore, classified as MFC, rather than NFC. Also, as there were no modifications made to the MFC, it should be classified additionally as a flocculated structure MFC according to Nechyporchuk et al. (2016b). Dilutions of 0.5, 1 and 2 wt% for further use were obtained by the addition of tap water, followed by 2 min of rotor stator mixing at 12,000 min^{-1} (rpm) (Polytron PT 3000, Kinematica, Switzerland) and 5 min exposure to an ultrasonic bath. Before further measurements, the dilutions were let to rest for at least 1 h. As a reference for flow curve measurements, a standard oil was used (Brookfield, fluid 1000, 985 mPas at 25 °C).

Imaging

For imaging, the MFC suspension was diluted to 0.5 wt% and an equivalent of 5 wt%, based on dry weights, of carboxymethyl cellulose (Finnfix10, CP Kelco, Finland) was added as 1 wt% solution, prior to the above described mixing and ultrasonication. For optical microscopy (Axio Imager.M2 m, Zeiss, Switzerland), one drop of suspension was placed between two glass slides. Another sample of this suspension was frozen in liquid nitrogen and then freeze dried using an automated system (Alpha 1-2 LD Freeze Dryer, Martin Christ Gefriertrocknungsanla-gen GmbH, Germany). A piece was torn out of the
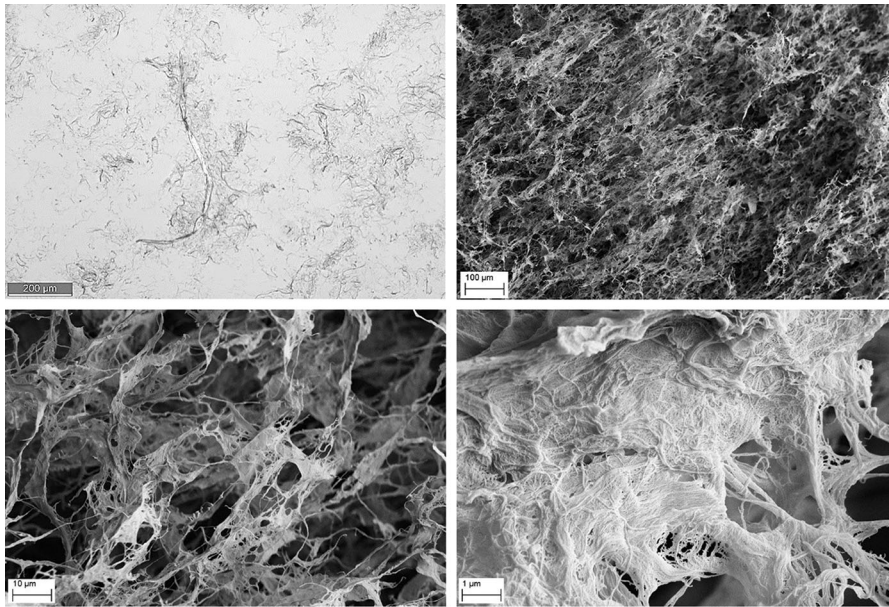
Fig. 1 Optical microscopy image of MFC suspension at 0.5 wt% (top left), and SEM images of freeze-dried aerogels from 0.5 wt% suspensions at increasing magnifications (top right), (bottom left) and (bottom right). Some left over coarse fibres are apparent, as well as some individual and isolated fibrils

aerogel and mounted on a support, so that the internal MFC aerogel structure could be imaged by SEM (Sigma VP, Zeiss, Switzerland) after being sputtered with gold (8 nm).

Rheological measurements

All the measurements were performed on an MCR 300 rheometer (Anton Paar, Austria) at 20 °C. Four different measurement systems were used, whereas all are based on a wide gap, cylinder and cup geometry. The first system is the CC27 ($d_{cup} = 28.92$ mm, $d_{bob} = 26.66$ mm), as it is supplied by the manufacturer (Anton Paar). The second system is also a CC27 system, but both cup and bob were roughened using a rough, 100 grit-class abrasive sandpaper (RR). The dimensions of the bob and cup as well as the moment of inertia of the bob were updated in the software accordingly. The roughening process led to a patterning on the surface, consisting predominantly of circular grooves around the geometrical rotation axis. So, waviness instead of roughness was calculated according to ISO 25178 for the bob from five different images recorded with a confocal laser scanning microscope (LSM 5 Pascal, Zeiss, Switzerland). The waviness was 1.8 ± 0.3 µm. The third system is the CC17 system ($d_{cup} = 18.08$ mm, $d_{bob} = 16.66$ mm) from Anton Paar. The fourth system is a vane (six blades) in serrated (length profiled) cup system (vane: ST22-6V-16, $d_{vane} = 22$ mm, cup: CC27-SS-P, $d_{cup} = 28.88$ mm, profile depths = 0.5 mm, profile widths = 1.65 mm), also supplied by Anton Paar (VS).

All the MFC suspensions, as well as the viscosity standard oil were measured as triplicates, whereas each measurement within a triplicate was a separate filling. For a given dilution, several dilution make-downs were used throughout the work presented here, whereas the repeatability was checked in all cases (data not shown). The data are presented as average values from the triplicate measurements, and respective standard deviations.

Flow curves (viscosity η in dependence of the shear rate $\dot{\gamma}$) were recorded by performing an automated shear rate increase ramp from 0.01 to 1000 s^{-1}. 30 log-equidistant distributed point measurements were performed with automated acquisition time mode (minimal acquisition time is 15.2 s) and shear rate control.

As seen also by others, the flow curve of an MFC (or NFC and NCC) suspension typically consists of several, more or less distinct regions, showing

different dependencies (Iotti et al. 2011; Jia et al. 2014; Karppinen et al. 2012; Shafiei-Sabet et al. 2012). Therefore, a focus of this work was put on a more effective description of these regions, to enable a comparison of such flow curves quantitatively. Figure 2 shows a typical flow curve with two zones following a power law, divided by a transition showing a typical local minimum. At high shear rates, some measurements also showed an increase in viscosity with shear rate. This was attributed to non-laminar flow, observable as vortex in the cup. Such data points were omitted from the evaluation. Zone 1 and 2 are characterized by the two power law parameters of the Ostwald–de Waele fitting function according to

$$\eta_i = K_i \dot{\gamma}^{n_i - 1} \tag{1}$$

where η_i is the viscosity, K_i is the consistency coefficient and n_i the flow index of zone i.

Using the exponent $n - 1$ allows to compare it directly to data from other power law fluid descriptions based on stress, using the following form taken from the region beyond the yield stress τ_0 in the Herschel–Bulkley relation:

$$\tau = K \dot{\gamma}^n \quad \text{for} \quad \tau \gg \tau_0 \tag{2}$$

where τ is the shear stress (Lasseuguette et al. 2008). The data points for fitting in zone 1 were used up to

shear rates at which a sudden increase of the acquisition time was seen. This increase in rheometer automated equilibrium acquisition time is believed to be a signal that the material is undergoing a transition in rheological state as the time required to achieve a steady measurement increases. Likewise, the data points for zone 2 were selected after the acquisition time dropped significantly once again at a shear rate after the transition zone. Zone 1 is additionally described with its apparent end and a viscosity value $\eta_{0.02}$ (low shear viscosity) that is obtained by solving the respective power law fit for a shear rate of 0.02 s^{-1}. Zone 2 is described additionally with the apparent start point and a viscosity value η_{100} (closely after the transition between low shear and high shear viscosity) that is obtained by solving the power law function for $\dot{\gamma} = 100 \text{ s}^{-1}$. The transition zone is characterized by the ratio of the low shear viscosity and the high shear viscosity and the comparative *relative depth of the local minimum* $\Delta_{\min}$. The latter is a newly introduced parameterization that is thought to be an indication of how strongly the suspension is aggregated (flocculated) in the transition zone, e.g. previously reported, but not quantified accordingly, by Karppinen et al. (2012). It is calculated by first fitting a power law function according to Eq. (1) through $\eta_{0.02}$ and η_{100} and then interpolating it to the shear rate of the local minimum to get the *theoretical local*
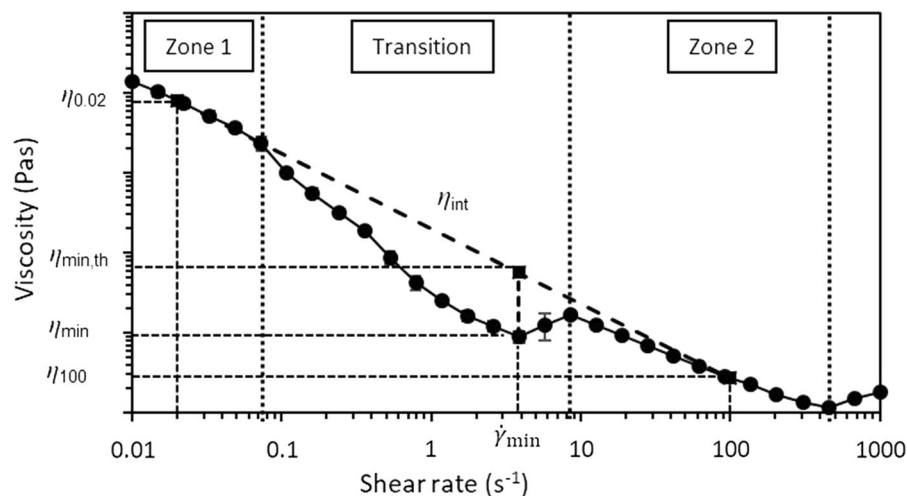

Fig. 2 Typical flow curve of an MFC suspension characterized in this work. There are three distinct regions; zones 1 and 2 following a power law, being divided by a transition region. Some combinations of measurement setups and suspension solid contents also showed a fourth zone where the viscosity

apparently seemed to increase. However, this was attributed to non-laminar flow, easily observable as vortex forming by the sample suspension in the cup. The parameters necessary for calculating the relative depth of the local minimum Δ_{min}, $\eta_{0.02}$ and η_{100} are indicated also

minimum viscosity [Eqs. (4), (5), (6)]. $\Delta_{\min}$ is then calculated as the difference between the theoretical local minimum viscosity and the actual viscosity at the local minimum, normalized by the theoretical local minimum viscosity [Eq. (3)],

$$\Delta_{\min} = \frac{\eta_{\min,th} - \eta_{\min}}{\eta_{\min,th}} \tag{3}$$

$$\eta_{\min,th} = K_{int}\dot{\gamma}_{\min}^{n_{int}-1} \tag{4}$$

$$n_{int} - 1 = \frac{\log(\eta_{100}/\eta_{0.02})}{\log(100/0.02)} \tag{5}$$

$$K_{int} = \frac{\eta_{0.02}}{0.02^{n_{int}-1}} \tag{6}$$

with $\eta_{\min,th}$ being the calculated viscosity at the shear rate of the local minimum $\dot{\gamma}_{\min}$ using the fitting function calculated from η_{100} and $\eta_{0.02}$ with the flow index n_{int} and consistency coefficient K_{int} at the zone interface of the transition, and $\eta_{\min}$ being the local minimum viscosity.

It should be mentioned that the interpretation of $\Delta_{\min}$ has some limits. When $\eta_{\min}$ is acquired in equilibrium (stable reading), then it may give a good indication of the aggregation in the suspension following the conclusions of Karppinen et al. (2012). Yet, the acquisition times in the transition zone can exceed the maximal acquisition time set by the rheometer software under certain situations (data not shown). In this case, $\eta_{\min}$ may be overestimated, and therefore $\Delta_{\min}$ underestimated.

Viscoelastic properties were determined by an amplitude sweep measurement at a frequency of 0.5 Hz. The automated, amplitude-controlled ramp was set from 0.001 to 1000% with 60 log-equidistant distributed point measurements and automated acquisition time mode (in practice, the acquisition time was seen to be around 25.5 s for all points in all measurements).

It was found that there is only a very short linear regime for the storage modulus (G') at very low shear stresses, respectively extremely small amplitudes (Fig. 3), so the maximal storage modulus G'_{max} was evaluated in this work, rather than the typically used plateau value. Analogously, the minimum of the phase angle, δ_{min}, was evaluated. As the loss modulus G'' typically showed some more extended linear regime (LV), the plateau value G''_{lin} was evaluated. MFC
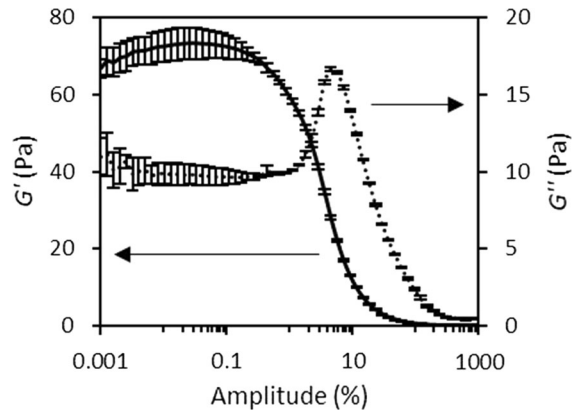

Fig. 3 Storage and loss modulus (G', G'') data of a 1 wt% MFC suspension measured with the CC27 geometry. The storage modulus data are represented with the full line on the left y-axis and the loss modulus data are represented with the dotted line on the right y-axis, respectively. Please note the different scales of both y-axis. The error bars indicate the standard deviation. It is apparent that the storage modulus is not linear, but goes through a maximum before the structure breakdown. The loss modulus is linear at low oscillation amplitudes and shows an increase before the structure breakdown

suspensions are known to behave like gels above certain concentrations, i.e. behaving like a viscoelastic solid ($G' > G''$) in a linear viscoelastic region (LVE), and after exceeding a critical shear stress, behaving like a viscoelastic liquid ($G' < G''$). Following (Moberg and Rigdahl 2012), the onset of the loss of linearity (Wu and Morbidelli 2001) was determined by the onset of the transformation from the viscoelastic solid to the viscoelastic liquid behaviour. Yet, in this work, the onset of the loss of linearity (LoL) was defined as the deformation at which the phase angle exceeded the minimal phase angle by 5%. Selecting the phase angle instead of the storage modulus to define the LoL was applied because the phase angle also includes the viscous behaviour of the material, i.e. the loss modulus:

$$\delta = \tan^{-1}\left(\frac{G''}{G'}\right) \tag{7}$$

The authors believe that in the case of a viscoelastic material, both moduli should be considered when discussing the structural response to a deformation, i.e. when undergoing shearing. Considering the storage modulus only may give an incomplete picture as the material naturally has a viscous response to the deformation, even at low deformations, i.e. in the
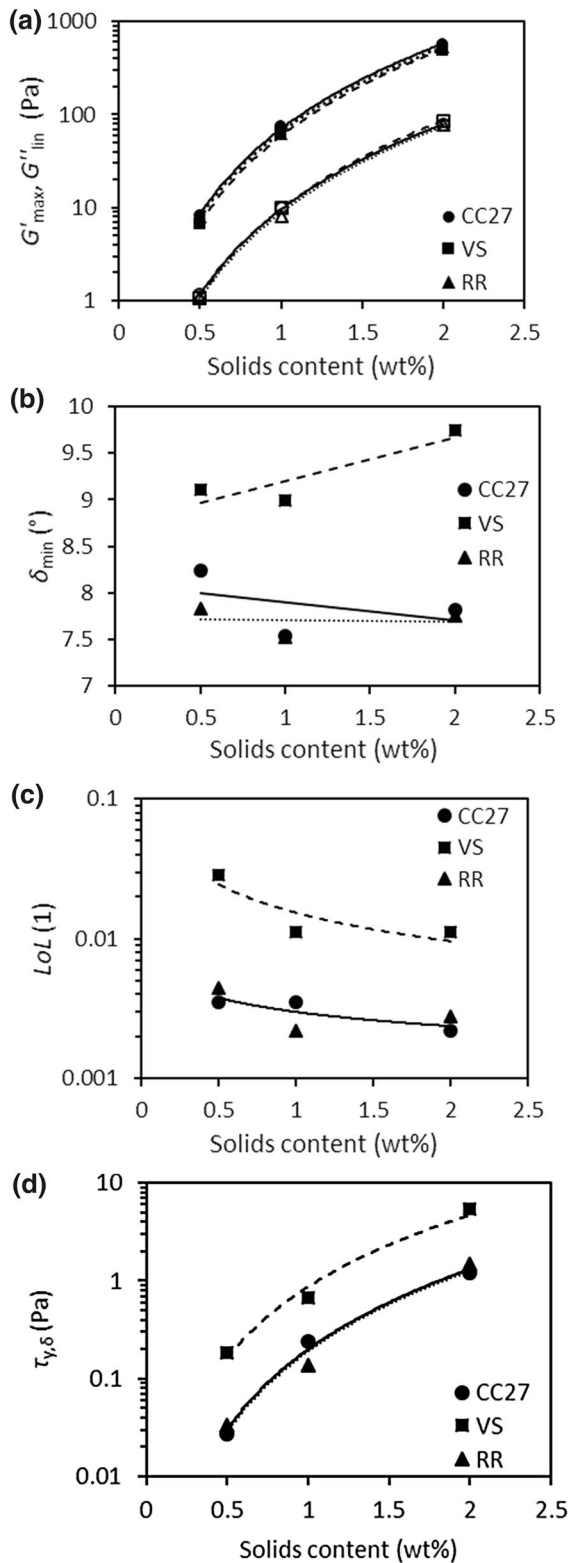
Fig. 4 Viscoelastic properties in dependence of the suspension solids content for the different measurement systems CC27: smooth setup, VS: vane in serrated cup, RR: roughened cup and bob, as shown in **a**–**d**. In graph **a**, the maximum storage modulus data are represented with the filled symbols and the linear loss modulus data are represented with the hollow symbols, respectively

LVE. It was, however, also found that there is a good correlation between the *LoL* determined as described above, and when determined using the onset of the loss of the storage modulus alone (data not shown). The dynamic yield stress in this work is defined as the stress at the *LoL*, $\tau_{y,\delta}$, as opposed to the static yield, τ_0, shown in Eq. (2).

Results

Graphs of the data that were used to derive the viscoelastic and flow curve parameters evaluated in this study, are provided in the "Supplementary Information S1".

Viscoelastic properties

Figure 4a shows the evolution of the storage and loss moduli (G'_{max} and G''_{lin}) in the linear viscous regime (LV) as a function of the MFC suspension solids content for the different measurement systems. The storage modulus is significantly larger than the loss modulus under all geometric conditions, and the moduli increase with increasing solids content of the MFC suspension. This is typically seen throughout the literature, e.g. (Baati et al. 2017; Moberg et al. 2017; Nechyporchuk et al. 2016b; Pääkkö et al. 2007). Looking at an independent power law fitting, $y = ax^b$, of the moduli y against solids content x data (Table 1), it is apparent from the parameters a and b that the measurement system has only a small influence on the trends.

Only few authors have investigated the impact of different measurement systems on viscoelastic properties of MFC suspensions, e.g. (Naderi and Lindström 2015; Saarinen et al. 2009), whereas only Naderi and Lindström (2015) have directly compared different cylinder and cup setups (smooth and profiled). Saarinen et al. (2009) found that the cone-plate setup leads

Table 1 Fitting function parameters of selected viscoelastic properties. The fitting function variable x is the solids content, and y is the fitted modulus property

System	Property (y) (Pa)	$y = ax^b$	
		a (Pa)	b
CC27	G'_{max}	73	2.9
VS	G'_{max}	61	3.0
RR	G'_{max}	63	3.1
CC27	G''_{in}	9.8	3.0
VS	G''_{lin}	9.8	3.1
RR	G''_{lin}	8.1	3.3

to a higher storage modulus plateau, compared to a plate-plate and a cylinder cone (CC27) system (all systems had a smooth surface). They argued that if wall slip (due to wall depletion) would be the dominant erroneous effect, then the data should be oppositely related to those observed. So, they attributed the observed effect to the gap size, whereby, in the cone-plate setup, the gap was too small in relation to residual fibres and/or fibril aggregates ("flocs"). In addition, Naderi and Lindström (2015) found that the storage as well as the loss moduli were smaller when measured with smooth CC surfaces compared to a profiled surface CC setup. This effect was attributed to the depletion layer. As the data in Fig. 4a do not show any of those effects, it may be hypothesized, that the gap size is sufficiently large, so that no blocking of coarse aggregates occurs on the one hand, and that potential side-effects on the other hand contribute only slightly in the initial viscoelastic region.

Figure 4b reveals that the minimum in phase angle (δ_{min}) is generally higher for the VS system compared to the CC27 and RR systems. As a higher phase angle means that the ratio of the loss and storage moduli is shifted more toward the loss modulus Eq. (7), the data indicate a more viscous, but still overall elastically dominated, behaviour of the MFC suspension when characterized by the VS system. Assuming the viscous behaviour to be a relative movement between fibres, i.e. a relocation of connection points (attractive inter-fibril interactions), and the elastic behaviour to be the stretching of the fibrils and/or fibrillar network, thus increasing the radius of gyration, the VS system seems to promote the relative movement of fibrils over that of

distortion. This hypothesis remains, however, to be proven, e.g. by adding another measurement technique that allows high resolution (spatial and temporal) velocity profiling of the MFC suspension near the edges of the vane blades.

When the oscillation amplitude (strain) becomes large enough, then the structure breaks down and the viscoelastic properties of the suspension change. As explained earlier, this is characterized by the *LoL* and the yield stress ($\tau_{y,\delta}$) in this work (Fig. 4c, d). For all systems, a trend is seen that higher solids contents decrease the *LoL* and increase $\tau_{y,\delta}$. Such a trend is also seen in the data presented by Jia et al. (2014), yet the authors did not describe the effect. The increase of the shear stress with the increasing solids content of the suspension can be explained easily by the increased number of fibrils and fibril contact points per unit volume of the suspension. However, the increased amount of fibril contact points also means that the length between the contact points becomes smaller. So, less strain is needed to create higher stress and such that the contacts break at lower strain and the system, therefore, starts to yield at a lower strain due to the greater induced stress.

A significantly increased limit of linearity and yield stress is seen for the VS system compared to the two others. Two reasons may be hypothesized for the later onset of the structure yielding for the VS systems. Either, the suspension structure actually collapses later as a function of strain in the VS system, or there is slip or a depletion layer effect occurring in the two other systems that is just wrongly interpreted as structure yielding. Figure 5 shows the typical phase angle data, exemplified by the 1 wt% MFC suspension. The higher value for δ in the LVE is apparent for the VS system, but also that the increase of δ as a function of shear stress is initially slower for the VS system. The very abrupt increase of the phase angle at lower stress (and deformation) seen for the CC and RR system can indicate a slip, depletion layer or a shear banding effect. As there is no indication for such an effect within the LVE for the other systems, it may be hypothesized that one of the potential effects is induced in the CC and RR systems, or at least enhanced by the precedent deformation.
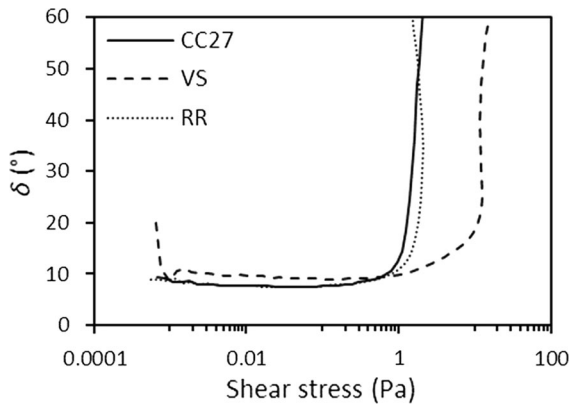
Fig. 5 Phase angle (δ) as a function of the shear stress (τ), derived from an amplitude sweep measurement performed on a 1 wt% MFC suspension with different measurement systems. The higher phase angle in the initial viscoelastic region, as well as the later and prolonged onset of the increase of the phase angle for the VS system are apparent

Flow curves

To verify that all measurement setups were initialized correctly, flow curves of a viscosity standard oil were recorded. Figure 6a shows the expected Newtonian behaviour and the viscosity value of about 1 Pas of the oil for all systems. This comparison is important, as it shows that, even though the VS and the RR systems are only relative systems, they actually report the correct absolute viscosity values and trends. Having this information makes it possible to attribute differences seen later in this work to the different material responses to the measurement setups, and not the measurement system itself. Please note also the lower shear rate limits for reliable measurements for the respective systems, provided by the rheometer supplier (Fig. 6a). Data of a given system that lie below the lower reliable detection limit on the curve should not be used. It is apparent, that the investigated measurement systems are not optimal for measuring low viscosity at low shear rates. Yet, as can be seen in Fig. 6b, viscosities of the investigated MFC suspensions were several orders of magnitude larger than 1 Pas at low shear rates, and, thus, generally very well within the detection limits for reliable measurement.

Several articles describe, that flow curves of MFC suspensions consist of two or three distinct regions, and attribute those to different suspension morphologies, i.e. different status of flocculation (Karppinen et al. 2012; Martoïa et al. 2015; Saarikoski et al. 2012;
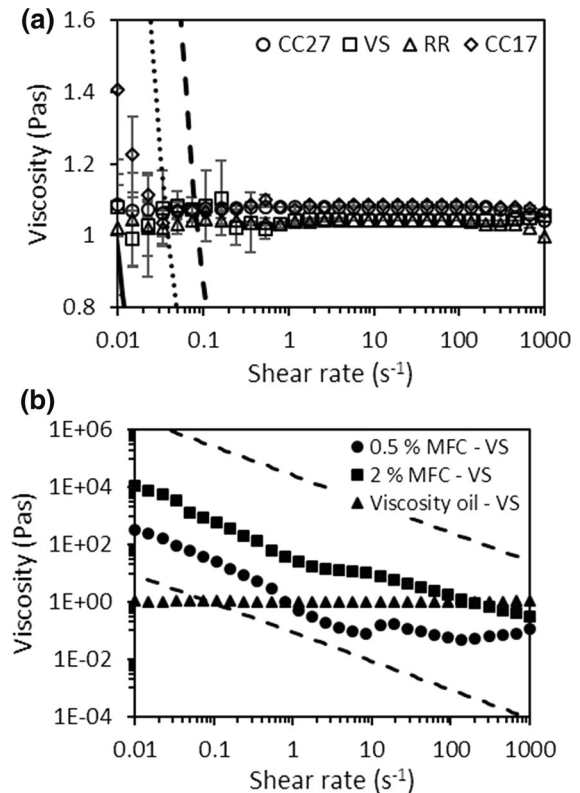

Fig. 6 Flow curves of a viscosity standard oil measured with the different measurement setups (a). The error bars represent the standard deviations. The lines mark the limits for reliable measurements provided by the machine supplier for the used setups (full: CC27 and RR, dashed: VS and dotted: CC17). Flow curve values that are below or close to the lower limit of detection should not be interpreted. The MFC suspension viscosity was well above these minimal detection limits, exemplified here with 0.5 and 2 wt% MFC measured with the VS system (b)

Saarinen et al. 2014). Some articles also describe such behaviour for NCC suspensions, though it is attributed to the transformation from isotropic to chiral nematic liquid crystalline phases (Shafiei-Sabet et al. 2012). Flow curves of NFC suspensions also consist of different regions, yet it seems that there is much less or no flocculation (Nechyporchuk et al. 2014). However, to obtain a real NFC according to the earlier provided definition, chemical modifications have to be applied, which inherently increase the charge density on the fibrils. This, in itself, will also change the rheological response of the system (Veen et al. 2015). Further work is planned to investigate the influence of the fibril widths on the rheological properties of MFC suspensions, without having an additional influence of a

changed surface charge. Karppinen et al. (2012) and Saarikoski et al. (2012) show that, at rest and very low shear rates, the MFC suspension is a network of fibrils. Increasing the shear rate leads to a "flocculation" of the fibrils. Up to a maximum, the floc size increases with increasing shear rate and "voids" (depleted, water-rich areas) form and grow. After reaching the maximum, the floc size decreases again and the voids disappear. It should be noted here that the term "floc" is loosely used to refer to papermaking terminology where fibres are seen to clump together in a bulky cooperative structure. However, shear induced structure, such as that seen here is more likely to be due to physical entanglement, such as occurs in polymer systems, rather than a colloidally defined floc. Martoïa et al. (2015) confirmed this floc behaviour also for enzymatic NFC, and it can be attributed to a competition between attractive and repulsive surface forces (Chaouche and Koch 2001) that is influenced by the shear rate and stress condition. Saarinen et al. (2014) found additionally that there can be significant solids depletion at low shear rates ("below the yield stress"), dominating the flow curve. Naturally, this depleted layer also is seen in terms of rapid shear thinning. In all the aforementioned publications smooth cylinder cup setups were used, with gap widths ranging from 0.5 to 2 mm. Also, the investigated MFC or NFC suspensions were very probably similar to the MFC suspension that was used here in our work. In the following discussions of the flow curves, the same models are assumed because of these likely similarities between the materials and methods used and those applied in this work. It should be noted that comparing alike types of nanocelluloses is important, as different types behave differently in rheological measurements. It seems that three major types with different rheological behaviour can be distinguished: modified [e.g. 2,2,6,6-tetramethylpiperidinyloxyl (TEMPO)-oxidized] and then fibrillated, mechanically fibrillated (including enzymatically pretreated) and crystalline cellulose. The main difference between the modified and the unmodified fibrillated materials is the increased surface charge, for example, due to the oxidation or the addition of polyelectrolytes. This increases the repulsive surface forces, and therefore works against flocculation (Martoïa et al. 2015; Moberg et al. 2017; Naderi and Lindström 2016; Veen et al. 2015). Crystalline celluloses typically also carry more surface charges than fibril-derived materials, and have

additionally a smaller aspect ratio and are stiff compared to fibrils, allowing them, for example, to form nematic structural phases (Shafiei-Sabet et al. 2012).

Figure 7 summarizes the properties of zone 1 of the flow curves of the different measurement systems and as a function of the suspension solids contents. It is apparent, that the end of zone 1, or the beginning of the transition region, strongly depends on the measurement system (Fig. 7a). Looking at the power law parameters (K_1, n_1) and the related low shear viscosity ($\eta_{0.02}$) reveals that the material in the VS system leads to significantly different results compared to the other systems (Fig. 7b–d). Also, the material in the RR system behaves differently, because the acquisition time data (not shown) indicate that there is no zone 1 in the RR setup measured flow curves, at least as we define it, i.e. no stabilized acquisition time. Due to this, no further evaluation of zone 1 properties according to the procedure described in the methods section was carried out using the RR system. However, it is apparent that the flow index n_1 would be negative before zone 2 starts for the RR system (n_1 would have been -0.13, -0.25 and -0.05 for 0.5, 1 and 2 wt%). A similar behaviour was described by Nechyporchuk et al. (2014), comparing smooth and rough surface cone-plate systems. Optical visualization revealed that there was wall slip on the smooth moving surface geometry, and a significant solids depletion layer on the rough, moving surface. They attributed the depletion ("water release") directly to the roughness and the deformation, since at the initial low shear rates, no water release was seen. This is in very good agreement with the data presented in this work. From the two smooth systems (CC27 and CC17), the smaller gap system CC17 shows slightly increased viscosity. This is initially unexpected because the depletion layer effect should become proportionally larger for a smaller gap (reducing the viscosity in the smaller gap), assuming a depletion layer thickness independent of the gap (Barnes 1995; Yoshimura and Prud'homme 1988). It could, however, be hypothesized that the depletion layer could not stabilize in the presence of fibril flocs. In other words, the flocculated structures may have been so large in comparison to the measurement gap, that physical bridging occurred between the rotating and static geometry (alike the observations made by Saarinen et al. (2009) in viscoelastic measurements). This then led to an
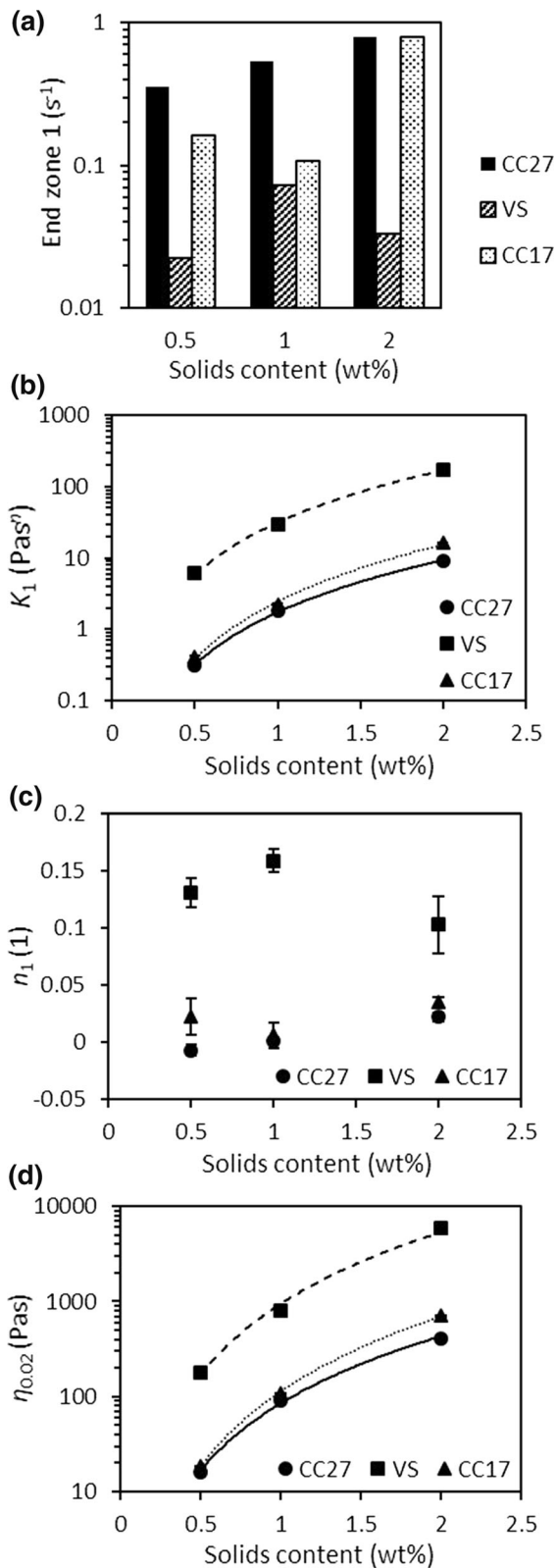
(a)

(b)

(c)

(d)

apparently increased viscosity, compared to the larger gap system (CC27). Following the earlier reasoning, it may be concluded, that the viscosity ($\eta_{0.02}$) data in Fig. 7d is dominated by a side-effect for the CC systems, and less pronounced in the VS system. Haavisto et al. (2015) find that flow indices close to 0 (and smaller than ca. 0.2) are a clear indication for slip induced by a depletion layer. So, following their argumentation, the here presented zone 1 data of the VS system with flow indices between 0.10 and 0.16 may still be dominated by the presence of a depletion layer. It should be kept in mind, however, that depletion on a vane geometry may have different consequences for the contribution to artefacts as there is significantly less tangential surface area compared to complete concentric cylinder setups. Also, additional side effects like suspension fracture at the edges of the blades (Nechyporchuk et al. 2015) may be present in the VS system. So, without a direct observation of the flow dynamics of an MFC suspension in a VS system, the degree of susceptibility and the nature of potential measurement artefacts of the VS system remain unclear. Also, the transition region starts earlier for the VS system (Fig. 7a), indicating an earlier onset of flocculation because of a better shear transfer into the measurement gap, or a delay of the onset for the two CC systems due to slip, depletion or banding. As there is a constant, unidirectional shear in a flow curve experiment (strain deformation of the viscous suspension), the flow situation can be considered to be occurring outside the LVE, i.e. no longer dominated by elastic interactions. So, the conclusions drawn from the zone 1 flow curve behaviour (i.e. more pronounced side-effects for non-VS systems) are in good agreement with the observations made at the end of the LVE (onset of the increase of the phase angle).

With some exceptions, it seems that the end of zone 1 is shifted to higher shear rates when the solids content of the MFC suspension increases (Fig. 7a). This indicates that the flocculation that is attributed to the transition region is hindered by a higher fibril concentration. In conjunction with the increase of
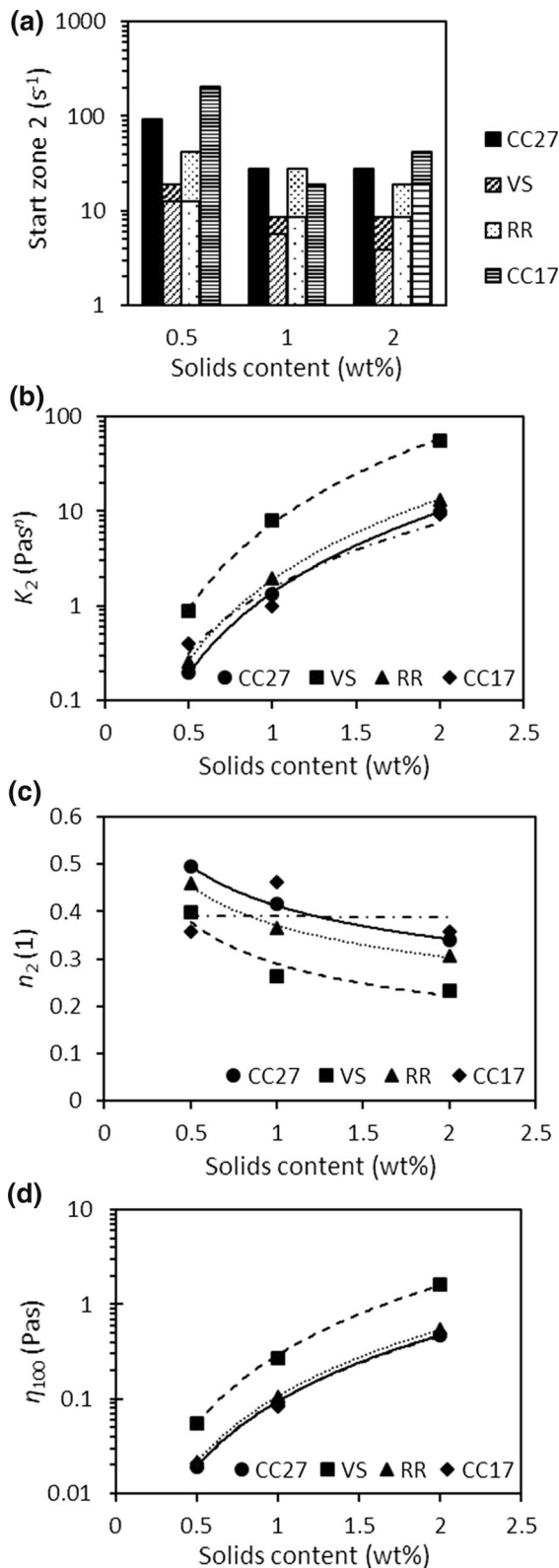
(a)

(b)

(c)

(d)

◄**Fig. 8** Description of zone 2 of the flow curve: start of zone 2 (**a**), power law parameters K_2 (**b**) and n_2 (**c**) and the interpolated viscosity at 100 s^{-1} (**d**). The lighter shaded bars in **a** show the earliest shear rate at which one of the triplicate measurements started the zone 2 power law behaviour. The difference of lighter and darker shaded bars of the same pattern is therefore a zone 2 onset deviation range

viscosity ($\eta_{0.02}$) with the solids content (Fig. 7d), it can be concluded that reorganization of the fibril network is hindered by a higher fibril concentration. This is rather straightforward, assuming that there are more connection points and more entanglements in a higher concentrated suspension (Iotti et al. 2011). Considering the standard deviations and the scatter of the flow indices (Fig. 7c), no clear trend, however, can be identified.

The overall trends in zone 2 appear alike the ones seen for zone 1, when looking at Fig. 8. The onset of zone 2 for the VS system happens at lower shear rates compared to all other systems (Fig. 8a) and the consistency coefficient (K_2) as well as the high shear viscosity (η_{100}) are highest (Fig. 8b, d). We can see that the relative difference between the VS and the other measurement systems is, however, smaller compared to the differences in zone 1 (Fig. 7b, d). The flow index of the VS system, though, is found to be smaller compared to the other systems (Fig. 8c). As in zone 1, an earlier onset of zone 2 for the VS system may indicate a better transmission/carry-over of the shear across the measurement gap. As reported by others, it is likely that the whole material in the measurement gap is sheared homogeneously at high shear rates (Nechyporchuk et al. 2014) with influences arising from depletion or other effects significantly suppressed. But apparently there are still some side-effects present overall as the zone 2 flow curves of the different systems are not identical. This is also supported by Kataja et al. (2017), who show that a depletion layer and/or solids content gradient layers remain present, even at high shear rates (volume flows).

Interestingly, the start of zone 2, which is the change from a strongly flocculated system to a more homogeneous system (Karppinen et al. 2012), is shifted to lower shear rates for higher solids contents of the suspension (Fig. 8a). Following the observation of Karppinen et al. (2012), that "voids" (fibril-free,

water-filled areas) are formed in the transition zone, it can be assumed that the size and volume fraction of these voids increase with decreasing solids content, as more water can be released from the gel structure. This then leads to a delay of the reorganization of the floc structure into the more homogeneous dispersion. In contrast to the flow indices of zone 1 (Fig. 7c), the ones of zone 2 (n_2, Fig. 8c) follow a power law trend as a function of solids content (Table 2) and become smaller with increasing solids content of the suspension. This means that a higher solids content leads to a stronger shear thinning behaviour at increased shear rates. It is assumed that in zone 2, the suspension structure becomes more homogeneous (Haavisto et al. 2015; Karppinen et al. 2012) and/or more aligned (Iotti et al. 2011) with increasing shear rate. This will lead to less dynamic entanglements and therefore an eased flow. However, this does not preclude cooperative motion being considered to account for strong shear thinning, which has been seen and modelled in generalized particulate suspension systems (Toivakka and Eklund 1994, 1995). Assuming that

entanglements are the major contribution to the dynamic viscosity of an MFC suspension, then this means that at very high shear rates (with respect to the shear rate range investigated in this study) the viscosity does not depend as strongly on the solids content, because the structure is less randomly entangled anyway, though the cooperative motion hypothesis may well be stronger at higher solids content (Toivakka and Eklund 1994). However, at lower shear rates, still in zone 2, the viscosity is more strongly dependent on solids content because there are still entanglements undergoing dynamic formation and break-up, and their dynamic interaction rate depends on the particle–particle encounters, and so, inevitably, on solids content. This hypothesized mechanism would then explain the stronger shear thinning behaviour at higher solids contents as the change from dynamic contacts towards stabilized homogeneous or cooperative flow occurs rapidly. The increase of the overall viscosity in zone 2 (η_{100}) with the suspension solids content (Fig. 8d) is still related to an increased amount of total contact points and entanglements (Iotti et al. 2011), and, thus, still increases with increasing solids content.

The transition zone depth, $\Delta_{\min}$, is about the same for all systems where a local minimum was identified (Fig. 9a). This may indicate, that the same maximum degree of flocculation is achieved in all systems. However, depending on the measurement setup, this happens at different shear rates (local minimum, Fig. 9b). The CC27 system did not show a clear minimum, even though the flow curve and the acquisition time data indicate a transition zone. It may be that the flocs in this system become as big as the measurement gap, or protrude into the transition wall and void regions, and therefore lead to blocking, interpreted as increased viscosity. The transition zone depth decreases with the solids content of the MFC suspension. This is in good agreement with the observations made in zone 2, assuming bigger depleted voids and higher void shares also lead to a larger drop in viscosity.

Table 2 Fitting function parameters of selected flow curve properties. The fitting function variable x is the solids content, and y is the fitted property

System	Property (y)	$y = ax^b$	
		a	b
CC27	K_1	1.8	2.3
VS	K_1	30	2.5
CC17	K_1	2.2	2.9
CC27	$\eta_{0.02}$	90	2.2
VS	$\eta_{0.02}$	809	2.8
CC17	$\eta_{0.02}$	108	2.7
CC27	K_2	1.3	2.9
VS	K_2	8.0	2.8
RR	K_2	2.0	2.8
CC17	K_2	1.1	3.1
CC27	n_2	0.41	− 0.27
VS	n_2	0.29	− 0.43
RR	n_2	0.37	− 0.30
CC17	n_2	0.39	0
CC27	η_{100}	0.09	2.4
VS	η_{100}	0.27	2.6
RR	η_{100}	0.11	2.4
CC17	η_{100}	0.09	2.5

Conclusions

The aim of this work was to investigate the effects of different shear rheometer measurement setups on the observed rheological properties of MFC suspensions.
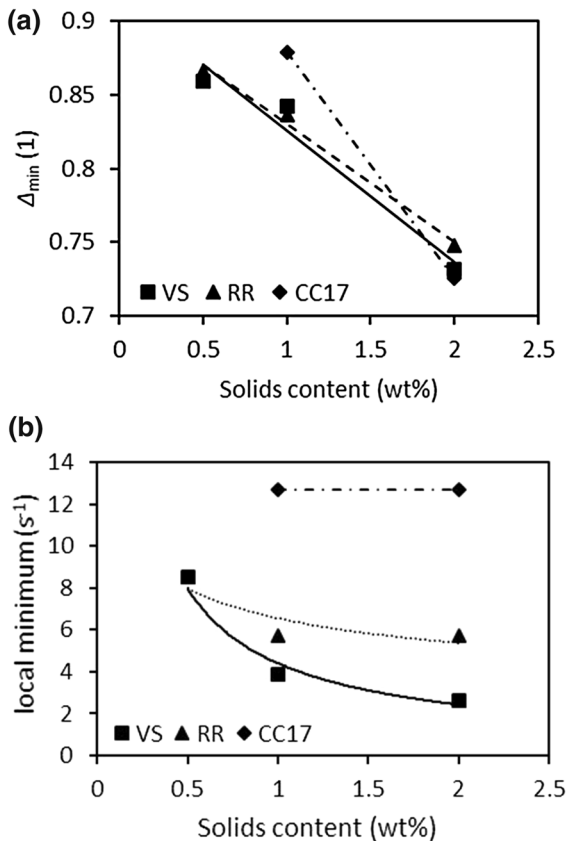
Fig. 9 Description of transition zone properties: **a** relative depth of the local minimum, and **b** the shear rate where the relative depth of the local minimum appears. The dotted lines are just for visual guidance and are not actual fits

Commonly used as well as newly proposed descriptors of viscoelastic and flow curve data were compared. Also, the potential mechanisms leading to the different results were proposed and discussed in relation to current morphological models of MFC suspensions.

The viscoelastic measurements have shown that at very low deformations up to the elastic modulus maximum, where elastic interactions dominate the suspension response, commonly observed rheometric-induced side-effects (artefacts) like slip, solids depletion at the wall or shear banding only have a minor impact on the results. This finding of course may well be limited to the settings and conditions used in this study. It was seen that different commonly used measurement systems delivered very similar results. There is an indication, however, that the vane system with serrated wall cup (VS) is the least perturbation affected system. When the oscillation amplitude

becomes larger, it seems that side-effects are induced in the smooth surface cylinder in cup (CC) and surface roughened (RR) setups, indicated by a very fast increase of the viscoelastic phase angle, and particularly an earlier onset of this increase compared to the VS system.

The flow curve data support the findings from the viscoelastic measurements. The lower viscosities and the later onsets of the transition region, respectively into zone 2, seen for the CC and RR systems compared to the VS system, indicate the presence of artefacts acting as side-effects. These observations are also well supported by recent publications where velocity profiling techniques reveal the flow dynamics of sheared MFC suspensions. The results presented here have shown that it is very likely that the VS system is much less susceptible to side-effects also in this shear regime, and therefore should be preferred when characterizing MFC suspensions. Yet further studies, specifically on a wide range of MFC suspensions and a variety of vane-based setups, involving velocity profiling methods, would be needed for verification of this hypothesis before considering it a generalization.

The trends of rheological parameters as a function of the MFC suspension solids content were also investigated. Despite the presence of side-effects that are suspected to be present in the CC and RR systems, most of the properties followed the same trends across the various geometries, independent of the measurement system used.

To be able to compare rheological data quantitatively, like the ones presented here, the obtained data need to be parameterized accordingly. The relevance in describing, for example, the onset points of different zones in the flow curves, or the limit of linearity in viscoelastic measurements, has been demonstrated here.

With this work as a basis, further investigations on the rheology of MFC suspensions as a function of MFC type and material properties are planned, providing further insight concerning the relationship between rheology and the morphology of MFC fibrillar material in suspension.

References

Baati R, Magnin A, Boufi S (2017) High solid content production of nanofibrillar cellulose via continuous extrusion. ACS Sustain Chem Eng 5:2350–2359. https://doi.org/10.1021/acssuschemeng.6b02673

Barnes HA (1995) A review of the slip (wall depletion) of polymer solutions, emulsions and particle suspensions in viscometers: its cause, character, and cure. J Nonnewton Fluid Mech. https://doi.org/10.1016/0377-0257(94)01282-M

Chaouche M, Koch DL (2001) Rheology of non-Brownian fibres with adhesive contacts. J Rheol 42:369–382. https://doi.org/10.1122/1.1343876

Desmaisons J, Boutonnet E, Rueff M, Dufresne A, Bras J (2017) A new quality index for benchmarking of different cellulose nanofibrils. Carbohy Polym. https://doi.org/10.1016/j.carbpol.2017.06.032

Dimic-Misic K, Maloney TC, Gane PAC (2015) Defining a strain-induced time constant for oriented low shear-induced structuring in high consistency MFC/NFC-filler composite suspensions. J Appl Polym Sci. https://doi.org/10.1002/app.42827

Dimic-Misic K, Rantanen J, Maloney TC, Gane PA (2016) Gel structure phase behavior in micro nanofibrillated cellulose containing in situ precipitated calcium carbonate. J Appl Polym Sci. https://doi.org/10.1002/app.43486

Dimic-Misic K, Maloney T, Liu G, Gane P (2017) Micro nanofibrillated cellulose (MNFC) gel dewatering induced at ultralow-shear in presence of added colloidally-unstable particles. Cellulose 24:1463–1481. https://doi.org/10.1007/s10570-016-1181-x

Haavisto S, Liukkonen J, Jäsberg A, Koponen A, Lille M, Salmela J (2011) Laboratory-scale pipe rheometry: a study of a microfibrillated cellulose suspension. In: PaperCon, Covington

Haavisto S, Salmela J, Jäsberg A, Saarinen T, Karppinen A, Koponen A (2015) Rheological characterization of microfibrillated cellulose suspension using optical coherence tomography. Tappi J 14:291–302

Haavisto S, Cardona MJ, Salmela J, Powell RL, McCarthy MJ, Kataja M, Koponen AI (2017) Experimental investigation of the flow dynamics and rheology of complex fluids in pipe flow by hybrid multi-scale velocimetry. Exp Fluids. https://doi.org/10.1007/s00348-017-2440-9

Iotti M, Gregersen OW, Moe S, Lenes M (2011) Rheological studies of microfibrillar cellulose water dispersions. J Polym Environ 19:137–145. https://doi.org/10.1007/s10924-010-0248-2

Jia X et al (2014) Rheological properties of an amorphous cellulose suspension. Food Hydrocolloids 39:27–33. https://doi.org/10.1016/j.foodhyd.2013.12.026

Kangas H, Lahtinen P, Sneck A, Saariaho AM, Laitinen O, Hellén E (2014) Characterization of fibrillated celluloses. A short review and evaluation of characteristics with a combination of methods. Nord Pulp Pap Res J 29:129–143. https://doi.org/10.3183/NPPRJ-2014-29-01-p129-143

Karppinen A, Saarinen T, Salmela J, Laukkanen A, Nuopponen M, Seppälä J (2012) Flocculation of microfibrillated cellulose in shear flow. Cellulose 19:1807–1819. https://doi.org/10.1007/s10570-012-9766-5

Kataja M, Haavisto S, Salmela J, Lehto R, Koponen A (2017) Characterization of micro-fibrillated cellulose fiber suspension flow using multi scale velocity profile measurements. Nord Pulp Pap Res J 32:473–482. https://doi.org/10.3183/NPPRJ-2017-32-03-p473-482

Kumar V, Nazari B, Bousfield D, Toivakka M (2016) Rheology of microfibrillated cellulose suspensions in pressure-driven flow. Appl Rheol 26:43534. https://doi.org/10.3933/ApplRheol-26-43534

Lasseuguette E, Roux D, Nishiyama Y (2008) Rheological properties of microfibrillar suspension of TEMPO-oxidized pulp. Cellulose 15:425–433. https://doi.org/10.1007/s10570-007-9184-2

Lauri J, Koponen A, Haavisto S, Czajkowski J, Fabritius T (2017) Analysis of rheology and wall depletion of microfibrillated cellulose suspension using optical coherence tomography. Cellulose. https://doi.org/10.1007/s10570-017-1493-5

Martoïa F, Perge C, Dumont PJJ, Orgéas L, Fardin MA, Manneville S, Belgacem MN (2015) Heterogeneous flow kinematics of cellulose nanofibril suspensions under shear. Soft Matter 11:4742–4755. https://doi.org/10.1039/c5sm00530b

Martoïa F, Dumont PJJ, Orgéas L, Belgacem MN, Putaux JL (2016) Micro-mechanics of electrostatically stabilized suspensions of cellulose nanofibrils under steady state shear flow. Soft Matter 12:1721–1735. https://doi.org/10.1039/C5SM02310F

Moberg T, Rigdahl M (2012) On the viscoelastic properties of microfibrillated cellulose (MFC) suspension. Annu Trans Nord Rheol Soc 20:123–130

Moberg T et al (2017) Rheological properties of nanocellulose suspensions: effects of fibril/particle dimensions and surface characteristics. Cellulose 24:2499–2510. https://doi.org/10.1007/s10570-017-1283-0

Moon RJ, Martini A, Nairn J, Simonsen J, Youngblood J (2011) Cellulose nanomaterials review: structure, properties and nanocomposites. Chem Soc Rev 40:3941–3994. https://doi.org/10.1039/C0CS00108B

Naderi A, Lindström T (2015) Rheological measurements on nanofibrillated cellulose systems: a science in progress. In: Mondal MIH (ed) Cellulose and cellulose derivatives. Nova Science Publishers Inc., New York, pp 187–202

Naderi A, Lindström T (2016) A comparative study of the rheological properties of three different nanofibrillated cellulose systems. Nord Pulp Pap Res J 31:354–363. https://doi.org/10.3183/NPPRJ-2016-31-03-p354-363

Naderi A, Erlandsson J, Sundström J, Lindström T (2016) Enhancing the properties of carboxymethylated nanofibrillated cellulose by inclusion of water in the pre-treatment process. Nord Pulp Pap Res J 31:372–378. https://doi.org/10.3183/NPPRJ-2016-31-03-p372-378

Nazari N, Kumar V, Bousfield DW, Toivakka M (2016) Rheology of cellulose nanofibers suspensions: boundary driven flow. J Rheol 60:1151–1159

Nechyporchuk O, Belgacem MN, Pignon F (2014) Rheological properties of micro-/nanofibrillated cellulose suspensions: wall-slip and shear banding phenomena. Carbohydr Polym

112:432–439. https://doi.org/10.1016/j.carbpol.2014.05.092

Nechyporchuk O, Belgacem MN, Pignon F (2015) Concentration effect of TEMPO-oxidized nanofibrillated cellulose aqueous suspensions on the flow instabilities and small-angle X-ray scattering structural characterization. Cellulose 22:2197–2210

Nechyporchuk O, Belgacem MN, Bras J (2016a) Production of cellulose nanofibrils: a review of recent advances. Ind Crops Prod 93:2–25. https://doi.org/10.1016/j.indcrop.2016.02.016

Nechyporchuk O, Belgacem MN, Pignon F (2016b) Current progress in rheology of cellulose nanofibril suspensions. Biomacromolecules 17:2311–2320. https://doi.org/10.1021/acs.biomac.6b00668

Pääkkö M et al (2007) Enzymatic hydrolysis combined with mechanical shearing and high-pressure homogenization for nanoscale cellulose fibrils and strong gels. Biomacromolecules 8:1934–1941. https://doi.org/10.1021/bm061215p

Padberg J, Bauer W, Gliese T (2016) The influence of fibrillation on the oxygen barrier properties of films from microfibrillated cellulose. Nord Pulp Pap Res J 31:548–560. https://doi.org/10.3183/NPPRJ-2016-31-04-p548-560

Pahimanolis N et al (2013) Nanofibrillated cellulose/carboxymethyl cellulose composite with improves wet strength. Cellulose 20:1459–1468

Saarikoski E, Saarinen T, Salmela J, Seppälä J (2012) Flocculated flow of microfibrillated cellulose water suspensions: an imaging approach for characterisation of rheological behaviour. Cellulose 19:647–659. https://doi.org/10.1007/s10570-012-9661-0

Saarinen T, Lille M, Seppälä J (2009) Technical aspects on rheological characterization of microfibrillar cellulose water suspensions. Annu Trans Nord Rheol Soc 17:121–128

Saarinen T, Haavisto S, Sorvari A, Salmela J, Seppälä J (2014) The effect of wall depletion on the rheology of microfibrillated cellulose water suspensions by optical coherence tomography. Cellulose 21:1261–1275. https://doi.org/10.1007/s10570-014-0187-5

Schenker M, Schoelkopf J, Mangin P, Gane P (2016) Rheological investigation of complex micro and nanofibrillated cellulose (MNFC) suspensions: discussion of flow curves and gel stability. Tappi J 15:405–416

Shafiei-Sabet S, Hamad WY, Hatzikiriakos G (2012) Rheology of nanocrystalline cellulose aqueous suspensions. Langmuir 28:17124–17133. https://doi.org/10.1021/la303380v

Toivakka M, Eklund D (1994) Particle movements during the coating process. Nord Pulp Pap Res J 9:143–149. https://doi.org/10.3183/NPPRJ-1994-09-03-p143-149

Toivakka M, Eklund D (1995) Prediction of suspension rheology through particle motion simulation. In: TAPPI coating fundamentals symposium, Atlanta, GA. TAPPI Press, pp 161–177

Turbak AF, Snyder FW, Sandberg KR (1983) Microfibrillated cellulose, a new cellulose product: properties, uses, and commercial potential. J Appl Polym Sci 37:815–827

Veen SJ, Versluis P, Kuijk A, Velikov KP (2015) Microstructure and rheology of microfibril-polymer networks. Soft Matter 11:8907–8912. https://doi.org/10.1039/C5SM02086G

Wu H, Morbidelli M (2001) A model relating structure of colloidal gels to their elastic properties. Langmuir 17:1030–1036. https://doi.org/10.1021/la001121f

Yoshimura A, Prud'homme RK (1988) Wall slip corrections for Couette and parallel disk viscometers. J Rheol 32:53–67. https://doi.org/10.1122/1.549963